

Article

Facile Preparation of YVO_4 : RE Films and the Investigation of Photoluminescence

Taihui Chen ^{1,2}, He Zhang ^{1,2}, Zhihong Luo ^{1,2}, Jun Liang ^{1,2,*} and Xiaoli Wu ^{1,2,3,*} 

¹ Guangxi Key Laboratory of Optical and Electronic Materials and Devices, Guilin University of Technology, Guilin 541004, China; 15007805225@163.com (T.C.); zhang_xiao_he@126.com (H.Z.); luozhihong615@163.com (Z.L.)

² School of Materials Science and Engineering, Guilin University of Technology, Guilin 541000, China

³ Collaborative Innovation Center for Exploration of Hidden Nonferrous Metal Deposits and Development of New Materials in Guangxi, Guilin University of Technology, Guilin 541004, China

* Correspondence: 1991005@glut.edu.cn (J.L.); wuxl-2008@163.com (X.W.)

Abstract: Facile preparation of YVO_4 films was hydrothermally achieved within 1 h by using layered yttrium hydroxide ($\text{Y}_2(\text{OH})_5\text{NO}_3 \cdot n\text{H}_2\text{O}$) films as the sacrificial precursor in the presence of excess NaVO_3 at pH~8, without subsequent heat treatment. Detailed structures and optical properties of the products were obtained by using a combination of XRD, FT-IR, FE-SEM, HR-TEM, and PLE/PL techniques. The phase and morphological evolution from $\text{Y}_2(\text{OH})_5\text{NO}_3 \cdot n\text{H}_2\text{O}$ to YVO_4 was unveiled by varying the reaction time. Photoluminescence spectra showed that the Eu^{3+} doped YVO_4 films exhibited the characteristic emission of Eu^{3+} , with the transition ${}^5\text{D}_0$ - ${}^7\text{F}_2$ (614 nm, red) being the dominant; while Dy^{3+} activator doped YVO_4 films exhibited the characteristic emission of Dy^{3+} , with the transition ${}^4\text{F}_9/2$ - ${}^6\text{H}_{13/2}$ (575 nm, green) being the most dominant.

Keywords: YVO_4 film; layered yttrium hydroxide film; sacrificial precursor; anion exchange; photoluminescence



Citation: Chen, T.; Zhang, H.; Luo, Z.; Liang, J.; Wu, X. Facile Preparation of YVO_4 : RE Films and the Investigation of Photoluminescence. *Coatings* **2022**, *12*, 461. <https://doi.org/10.3390/coatings12040461>

Academic Editor: Alicia de Andrés

Received: 11 February 2022

Accepted: 24 March 2022

Published: 29 March 2022

Publisher's Note: MDPI stays neutral with regard to jurisdictional claims in published maps and institutional affiliations.



Copyright: © 2022 by the authors. Licensee MDPI, Basel, Switzerland. This article is an open access article distributed under the terms and conditions of the Creative Commons Attribution (CC BY) license (<https://creativecommons.org/licenses/by/4.0/>).

1. Introduction

In recent years, lanthanide compounds have received widespread attention as excellent luminescent materials useful in the development of new lighting/visualization technologies [1,2]. Among them, the rare-earth orthovanadate (YVO_4 : RE) is considered an attractive compound since it displays high quantum yield caused by the efficient energy transfer from the VO_4^{3-} ligand to RE^{3+} . Because of the continuous development of optoelectronic devices, the design and fabrication of luminescent films have become more and more important. In the present research, we proposed a methodology to produce red-emitting and green-emitting YVO_4 : RE films, which may find wide applications in various lighting and display areas including fluorescent lamps, white LEDs, FEDs, PDPs, FDPs and CRTs, among others [3,4].

At present, a variety of techniques for the preparation of the vanadate films are available. They include the calcination of the MOF (metal-organic framework) precursor [5], pulsed-laser deposition [6], microwave-assisted chemical deposition [7] and sol-gel/electrospinning process [8], among others. The chemical deposition and pulsed-laser deposition are convenient when thin films are prepared from powder. However, these methods require expensive equipment. Calcination of the MOF (metal-organic framework) precursor and the sol-gel/electrospinning process require complex steps and/or high heat treatment temperatures, which may cause the film to crack. In the present work, a low-temperature method was used to synthesize YVO_4 : RE films from Layered Yttrium Hydroxide (LYH) film as sacrificial template and NaVO_3 as an anion source. The phase and morphological evolution during the transformation of LYH to YVO_4 and photoluminescence properties of activated (Eu^{3+} and Dy^{3+}) doped YVO_4 films were investigated in detail.

The layered rare earth hydroxides (LRHs) are a new type of inorganic functional layered compounds, and the general formula of “251” typed LRH is $\text{RE}_2(\text{OH})_5(\text{A}^{m-})_{1/m} \cdot n\text{H}_2\text{O}$ (RE = Rare-earth elements; A = Cl or NO_3). The structure of “251” typed LRH is constructed via alternative stacking of the hydroxide main layers composed of $[\text{Ln}(\text{OH})_7\text{H}_2\text{O}]$ and $[\text{Ln}(\text{OH})_8\text{H}_2\text{O}]$ coordination polyhedral and interlayer NO_3^- free anions along the *c*-axis ([001] direction) [9,10]. Because of their special layered structure and properties of rare-earth elements, the “251” typed LRHs have attracted extensive attention since they were first reported in 2006 [11]. In the past several years, different aspects of the “251” typed LRHs have been studied including the interlayer anion exchange capacity [10–15], catalytic performance of intercalated products [11,14,15], exfoliation of bulk crystals into nanosheets [16–18], photoluminescence [9,10,19–21], enhancement of luminescence [22–29], and the self-assembly of functional films [29–34]. Also, because of their composition and structure, a significant amount of research has been performed to study, photoluminescence properties of the “251” typed LRH. However, poor photoluminescence has been observed [9,10,19–21]. This low performance can be attributed to the presence of hydroxyl, crystal water, and nitrate groups in the LRH structure, that provide channels for nonradiative relaxation. The most common method used to achieve photoluminescence optimization, consists of inserting inorganic [21] or organic anions [25,26] via interlayer anion exchange to sensitize activators in the host layer. However, this method presents some limitations because the quenching groups are still present in the structure. Another way to enhance photoluminescence by doping the LYH and LGdH matrix with subsequent calcination to remove the quenching groups and form cubic $\text{Y}_2\text{O}_3:\text{RE}/\text{Gd}_2\text{O}_3:\text{RE}$ [16,19,22–24,31,32]. The heat treatment also requires high temperatures ($>550^\circ\text{C}$). Thus, in this optimization method, production of a flat film without cracks is still a challenge. In 2016, $(\text{Y}_{1-x}\text{Eu}_x)\text{PO}_4$ was successfully synthesized by using $(\text{Y}_{1-x}\text{Eu}_x)_2(\text{OH})_5\text{NO}_3 \cdot n\text{H}_2\text{O}$ as the sacrificial template and NaH_2PO_4 as an anion source [35]. However, high temperatures (600–1000 °C) were also required to produce the target $(\text{Y}_{1-x}\text{Eu}_x)_2\text{PO}_4$ phase. Still, it provides a theoretical basis for the design and preparation of various rare-earth materials. To the best of our knowledge, electrodeposited “251” typed LRH films have not been utilized as a precursor template to synthesize REVO_4 films at low temperatures, and without the need of further heat treatment. We believe that this strategy may attract wide research interest and result in the practical application of “251” typed LRHs.

2. Experiment

Materials: The rare-earth source of $\text{Y}(\text{NO}_3)_3 \cdot 6\text{H}_2\text{O}$ (99.5% pure), $\text{Eu}(\text{NO}_3)_3 \cdot 6\text{H}_2\text{O}$ (99.9% pure), $\text{Dy}(\text{NO}_3)_3 \cdot 6\text{H}_2\text{O}$ (99.9% pure) and Sodium metavanadate (NaVO_3 , 99.9% pure) were purchased from Shanghai Macklin Biochemical Co., Ltd., Shanghai, China. The indium tin oxide (ITO) glass (sheet resistance: $\leq 5 \Omega$) were obtained from Xiang Cheng Technology Ltd., Shenzhen, China. The platinum electrode and Ag/AgCl/saturated KCl electrode were purchased from Tianjin Ida Technology Co. Ltd., Tianjin, China.

Synthesis: The three-electrode cell system was used to prepare the $\text{Y}_2(\text{OH})_5\text{NO}_3 \cdot n\text{H}_2\text{O}$ film, in which the rare-earth nitrate solution as electrodeposition solution, ITO glass, platinum foil, and Ag/AgCl/saturated KCl were used as the working, counter, and reference electrodes, respectively. After the deposition, all films were cleaned with deionized water and dried at 60°C for 30 min. For the synthesis of the activator doped system $(\text{Y}_{1-x}\text{REpeatingH})_5\text{NO}_3 \cdot n\text{H}_2\text{O}$ (RE = Eu and Dy), the RE/(Y + RE) atomic ratio was tuned according to the doping amounts of activators, and then repeat the electrodeposition process. For the synthesis of YVO_4 films, 0.5 mol/L of NaVO_3 solution with pH value of 8 was prepared; then the LYH films were placed in the NaVO_3 solution, and the mixture was subjected to hydrothermal reaction at 100°C . Afterward, the prepared films were naturally cooled, washed several times with distilled water and ethanol, and then dried at 60°C for 30 min.

Characterization techniques: Phase identification was made via X-ray diffractometry (XRD, Model X'Pert PRO, PANalytical B.V., Almelo, The Netherlands) operated at 40 kV/40 mA nickel filtered using Cu-K α radiation ($\lambda = 0.15406$ nm) and a scanning speed of 15.0° 2 θ per minute. Fourier transform infrared spectroscopy (FT-IR, Model Spectrum RXI, Perkin-Elmer, Shelton, Connecticut) was conducted via the standard KBr method. The morphology and microstructure of the products were analyzed by field emission scanning electron microscopy (FE-SEM, Model JSM6380-LV, JEOL, Tokyo, Japan) and transmission electron microscopy (TEM, FEM-3000F, JEOL, Tokyo, Japan). The photoluminescence properties were measured on a FluoroMax-4 fluorescence spectrophotometer (HORIBA, Kyoto, Japan) using a 150 W Xe-lamp as the excitation source at room temperature.

3. Results and Discussion

3.1. Characterization of $Y_2(OH)_5NO_3 \cdot nH_2O$ (LYH) Film and YVO_4 Film

Figure 1a shows the XRD patterns of the precursor film and the anion-exchange film, respectively. The precursor film presents a series of (00 l) and (220) diffraction patterns characteristic of $Y_2(OH)_5NO_3 \cdot nH_2O$ compounds [10,12,13]. In addition, the diffraction peaks of the anion-exchange film can be assigned to pure tetragonal YVO_4 (PDF No.17-0341) [36]. Figure 1b shows the FT-IR spectra of the precursor and the anion-exchange films. In the precursor film spectrum, the absorption peak at ~ 1384 cm $^{-1}$ corresponds to uncoordinated NO $_3^-$ (ν_3) stretching [19–21,23,24], while the absorption band at ~ 3600 cm $^{-1}$ indicates OH $^-$ vibration [19–21,23,24]. Additionally, the absorption bands at ~ 3438 and ~ 1634 cm $^{-1}$ are attributable to the O-H stretching (ν_1 and ν_3) and H-O-H bending (ν_2) vibrations of hydration water, respectively [19–21,23,24]. The FT-IR analysis confirmed the existence of all the functional groups present in LYH. In the case of the anion-exchange film, the vibration peak of NO $_3^-$ and hydroxyl disappeared, while a strong absorption peak at 820 cm $^{-1}$ appeared. This peak can be assigned to stretch vibration (ν_3) originating from the V-O stretching vibration in VO $_4^{3-}$ [8,37]. However, the absorptions of H $_2$ O were still observable at 3412 cm $^{-1}$ and 1640 cm $^{-1}$, which indicated the presence of some hydration or surface-absorbed water molecules in the anion-exchange film rather than the coordinated H $_2$ O from the precursor LYH film [36]. These results demonstrated that the YVO_4 film was successfully synthesized by using $Y_2(OH)_5NO_3 \cdot nH_2O$ film as a precursor template and NaVO $_3$ as an anion source.

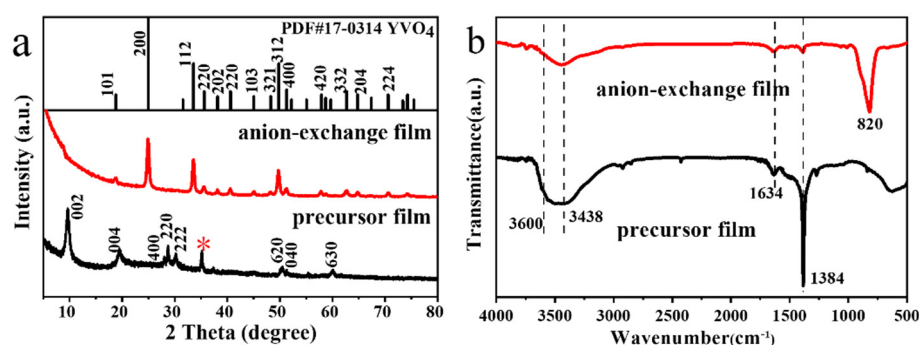


Figure 1. XRD patterns (a), FT-IR spectra (b) of the precursor film and anion-exchange film. The diffraction peaks of ITO glass were marked with *.

As shown in Figure 2a, the FE-SEM image indicated that the LYH precursor film crystallized as flower-like aggregates, which were assembled in nanosheets with different lateral and vertical arrangements and angles. As observed from the FE-SEM image in Figure 2b and the TEM image in Figure 2c, the YVO_4 film crystallized in structures like rice grains, which were totally different from those observed in the precursor template. Selected area electron diffraction (SAED, the inset of Figure 2c) yielded diffraction spots that correspond to the (200), (301) and (202) planes of tetragonal structured YVO_4 , indicating that the anion exchange film under observation is a well-crystallized single crystal. The iden-

tified (200), (301) and (202) diffractions displayed values of $d_{200} = 3.559 \text{ \AA}$, $d_{301} = 2.220 \text{ \AA}$ and $d_{202} = 2.357 \text{ \AA}$, respectively. These results were close to the values of $d_{200} = 3.574 \text{ \AA}$, $d_{301} = 2.228 \text{ \AA}$ and $d_{202} = 2.361 \text{ \AA}$ calculated from the XRD results, respectively. The (202) and (200) planes observed in the SAED pattern presented a dihedral angle of $\sim 48.7^\circ$, which was also close to the calculated value of $\sim 48.5^\circ$. High-resolution TEM (HR-TEM) analysis clearly resolved the lattice fringes of the LRH crystal, and a spacing of 0.354 nm properly corresponded to the (200) plane of the host layer (Figure 2d).

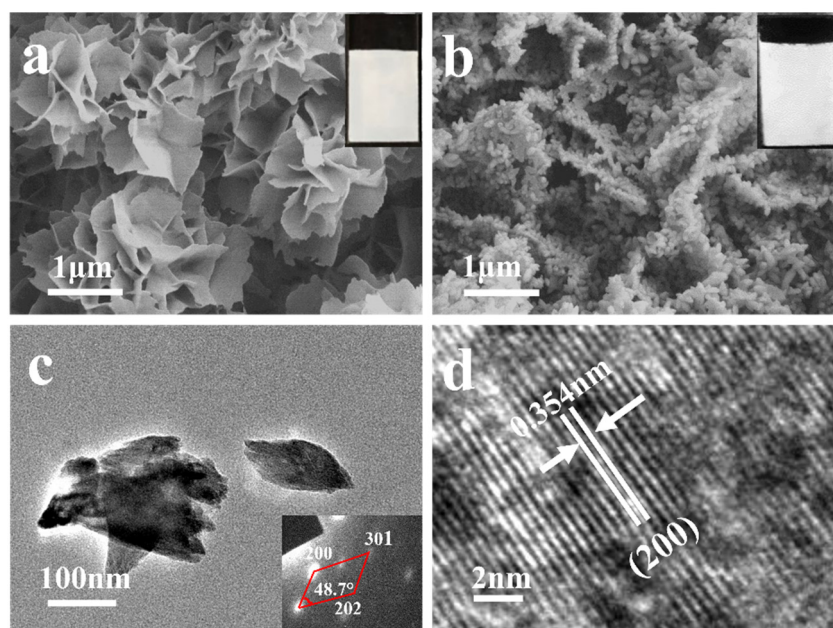


Figure 2. FE-SEM image of the $\text{Y}_2(\text{OH})_5\text{NO}_3 \cdot n\text{H}_2\text{O}$ film (a), FE-SEM image (b), TEM image (c), and HR-TEM image (d) of the YVO_4 film. The inset in (a) is the digital photograph of the $\text{Y}_2(\text{OH})_5\text{NO}_3 \cdot n\text{H}_2\text{O}$ film, The inset in (b) is the digital photograph of the YVO_4 film and the inset in (c) is the selected area electron.

3.2. Evolution of Phase and Morphology from LYH to YVO_4 upon Anion Exchange

Through a series of exploratory experiments, it was found that the concentration of NaVO_3 in the solution is the key factor affecting the phase and morphology of the exchanged products, and high concentrations of the anion source facilitated the reaction. To determine the phase and morphological evolution during the transformation from LYH to YVO_4 , different hydrothermal reactions were performed. For this purpose, we used 0.05 M NaVO_3 (with a fixed volume of 50 mL) as the anion source and LYH film as the precursor template. In addition, different reaction times were tested at pH of ~ 7.3 . Figure 3a compares the XRD patterns of the original LYH template and anion-exchange films at different reaction times. Data indicated that at a reaction time of 5 min , a mixture of phases was present. Herein, the peaks at 9.95° and 29.25° correspond to the characteristic diffraction of the (220) plane present in the LYH template. In addition, the diffraction peaks at 24.46° , 35.69° and 50.24° were well correlated with the (200), (112) and (312) planes of the YVO_4 phase, respectively. Obviously, LYH phase is the main phase in the mixture product. FT-IR (Figure 3b) showed that the absorption of uncoordinated NO_3^- at 1384 cm^{-1} and the absorption of VO_4^{3-} at 820 cm^{-1} were simultaneously observed when the reaction time was 5 min . With the increase in reaction time, the diffraction peaks of LYH became weaker, and the final YVO_4 anion exchange product was obtained until the reaction time reached 1 h . The corresponding FT-IR spectra of the exchanged products showed the weakened absorptions of hydroxyl and NO_3^- , and enhanced absorptions of VO_4^{3-} . Until the reaction time reached 1 h , the absorptions of hydroxyls and NO_3^- disappeared. According to the synthesis used in the present research, the phase conversion process from

LYH to YVO_4 may be described as follows: $\text{VO}_3^-(aq) + 2\text{OH}^-(aq) \rightarrow \text{VO}_4^{3-}(aq) + \text{H}_2\text{O}(aq)$. Subsequently, the coordinated hydroxyl and water present in $[\text{Y}_2(\text{OH})_5(\text{H}_2\text{O})_n]^+$ host layer were completely exchanged by VO_4^{3-} .

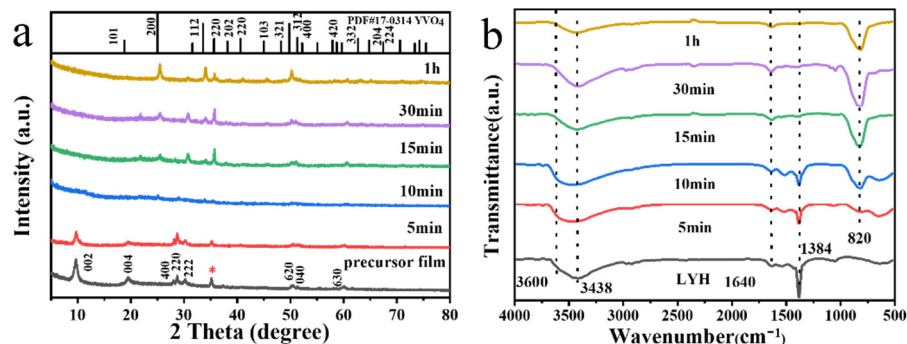


Figure 3. XRD patterns (a) and FT-IR spectra (b) of anion exchange films prepared with different reaction time. The diffraction peaks of ITO glass were marked with *.

The morphological evolution from LYH to YVO_4 can be observed in Figure 4. The sample with the reaction time of 5 min largely retained the LYH nanoplate-like morphology, among which some YVO_4 particles were found. The FE-SEM data showed that, with increasing reaction time, more LYH nanosheets were converted into YVO_4 spindle-shaped particles. When the reaction proceeded for 1 h, all the LYH nanosheets were completely transformed into YVO_4 spindle-shaped particles. This indicated that phase transition occurred a dissolution–reprecipitation mechanism.

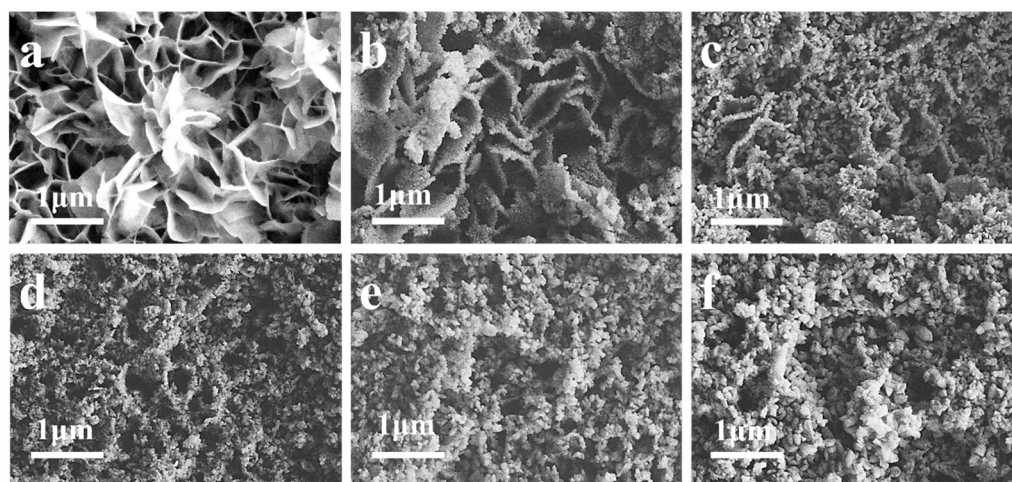


Figure 4. FE-SEM images of anion-exchange films prepared with different reaction times: 0 min (a), 5 min (b), 10 min (c), 15 min (d), 30 min (e) and 1 h (f).

3.3. Structure Characterization and Photoluminescence of Activators Doped YVO_4 Films

In the present research, two types of activated ion doped YVO_4 films (Eu^{3+} doped and Dy^{3+} doped) were prepared. Figure 5a shows the XRD results of the films obtained when reactions proceeded with different molar contents of Eu^{3+} . Data indicated that all the diffraction peaks can be well indexed to the tetragonal YVO_4 (PDF No.17-0341). As shown in Figure 5b, the body-centered tetragonal unit cell of YVO_4 consists of four units, where two sets of oxygen atoms, differing in the Y-O bond length, are coordinated to Y^{3+} to form the YO_8 dodecahedron. The derived cell parameters are summarized in Table 1. Compared with the standard YVO_4 film, the YVO_4 : Eu film presented a larger cell volume, which was ascribed to the increase in the RE-O bond length. This resulted from the replacement of smaller ionic radius of Y^{3+} with the larger Eu^{3+} (eight-fold coordination, 0.1019 nm

for Y^{3+} , 0.1066 nm for Eu^{3+}) and caused the direct crystallization of solid solution. The crystallite size assayed from the Scherrer equation via profile broadening analysis of the (200) diffraction, and the calculated values of the crystallite size are summarized in Table 1. Data shows that the crystalline size of YVO_4 : Eu nanoparticles gradually decreased with the increased doping amount of RE^{3+} ions.

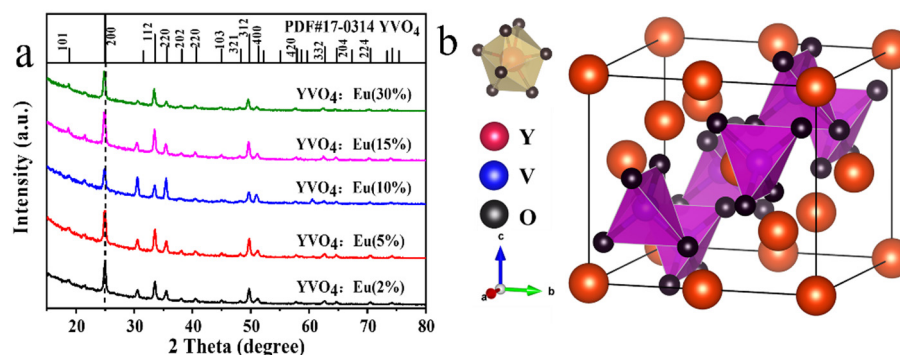


Figure 5. XRD patterns of the YVO_4 :Eu films with different molar doping concentration (a) and the schematic crystal structure of tetragonal REVO_4 (b). The Y^{3+} ligands of YVO_4 crystal structure are shown in the insets.

Table 1. The results of structure refinement and the crystalline sizes for YVO_4 : Eu^{3+} .

Samples	A = b (Å)	c (Å)	V (Å ³)	Crystalline Sizes (nm)
YVO_4 : Eu (2%)	7.100	6.259	315.516	24.51
YVO_4 : Eu (5%)	7.121	6.288	318.856	23.20
YVO_4 : Eu (10%)	7.137	6.304	321.105	21.73
YVO_4 : Eu (15%)	7.160	6.295	322.717	21.01
YVO_4 : Eu (30%)	7.163	6.315	324.014	20.46

The photoluminescence excitation (PLE) spectra of the YVO_4 : Eu^{3+} films observed by monitoring the red emission of Eu^{3+} at 614 nm consisted of a strong and broad excitation band ranging from ~280 to 320 nm (Figure 6a), which was attributed to the energy transfer from VO_4^{3-} to Eu^{3+} [38]. The molecular orbital theory suggests that the absorption band was overlapped by the charge electron transitions of VO_4^{3-} ion from the $^1\text{A}_2(^1\text{T}_1)$ ground state to the $^1\text{E}(^1\text{T}_2)$ excited state at 290 nm and $^1\text{A}_1(^1\text{E})$ excited state at 308 nm [36]. Negligible peaks located at 396 nm and 466 nm were observed, which resulted from the general $^7\text{F}_{0,1-5}\text{L}_6$ and $^7\text{F}_{0,1-5}\text{D}_2$ transitions of Eu^{3+} , respectively. Upon UV excitation at 290 nm, the photoluminescence (PL) spectra of the YVO_4 : Eu^{3+} films (Figure 6b) exhibited transitions from the $^5\text{D}_0$ excited state to the $^7\text{F}_j$ ($j = 1, 2, \text{ and } 3$) ground states of Eu^{3+} ranging from 500 to 650 nm, with the transition $^5\text{D}_0 \rightarrow ^7\text{F}_2$ (614 nm, red emission) being the most dominant [39,40]. According to the Judd-Ofelt parity rule [41,42], the relative intensity of emission peaks is closely related to the transition of excited electrons to different energy levels and the coordination environment of Eu^{3+} . The intensity of the $^5\text{D}_0 \rightarrow ^7\text{F}_2$ electric dipole transition is greater than that of the $^5\text{D}_0 \rightarrow ^7\text{F}_1$ magnetic dipole transition, indicating the activator Eu^{3+} occupies a low-symmetry site in the lattice. As shown in Figure 6b, the optimal concentration of doped Eu^{3+} was 10 mol (%); over-doping led to the concentration quenching of luminescence via cross-relaxation mechanism. Figure 6c,d show the excitation and emission spectra of YVO_4 : Dy^{3+} , respectively. By monitoring the emission of Dy^{3+} at 573 nm, it was observed that the PLE spectra of the YVO_4 : Dy^{3+} films exhibited a strong and broad band ranging from 280–310 nm, which was also associated with the efficient energy transfer from VO_4^{3-} to Dy^{3+} . Moreover, the peaks located at 350–500 nm were attributed to the $^4\text{F}_{9/2-6}\text{H}_{15/2}$ and $^4\text{F}_{9/2-6}\text{H}_{13/2}$ intra-transitions of Dy^{3+} (Figure 6c). Upon the excitation at 290 nm, the emission spectra of the YVO_4 : Dy^{3+} films were composed of two bands centered at ~483 nm (blue emission) and 573 nm (green emission, dominant),

which corresponded to the ${}^4F_{9/2}-{}^6H_{15/2}$ and ${}^4F_{9/2}-{}^6H_{13/2}$ intra-transitions of Dy^{3+} , respectively. Data in Figure 6d indicated that the optimal doped Dy^{3+} concentration was 5 mol (%). Additionally, the $(Y_{0.90}Eu_{0.05})VO_4$ and $(Y_{0.95}Dy_{0.05})VO_4$ films exhibited vivid red and bright green emissions under UV excitation at 254 nm.

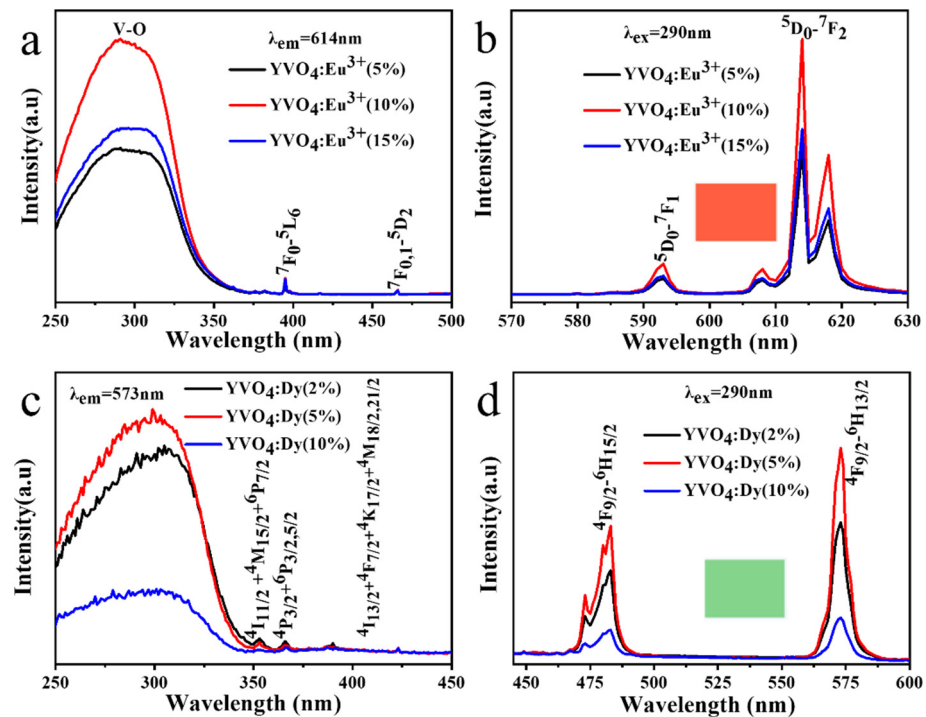


Figure 6. The excitation spectra (a) and emission spectra (b) of $Y_{1-x}Eu_xVO_4$ films prepared for 1 h, excitation spectra (c) and emission spectra (d) of $Y_{1-x}Dy_xVO_4$ films prepared for 1 h. Insets in (b,d) show red emission and green emission of the $(Y_{0.90}Eu_{0.10})VO_4$ film and $(Y_{0.95}Dy_{0.05})VO_4$ film under the UV excitation at 254 nm, respectively.

4. Conclusions

The rapid preparation of YVO₄ films was successfully performed via anion exchange reaction by using the electrodeposited LYH films as a precursor template and NaVO₃ as anion source at pH ~7.3, without further heat treatment. The phase evolution from LYH to YVO₄ was systematically studied, and the morphological evolution from flower-like LYH nanosheets to YVO₄ spindle-shaped particles indicated that a dissolution-reprecipitation mechanism occurred. Photoluminescence showed that YVO₄:Eu³⁺ films and YVO₄:Dy³⁺ films exhibited characteristic emissions depending on the RE³⁺. In addition, the optimal concentrations of doped Eu³⁺ and Dy³⁺ were determined as 10 mol (%) and 5 mol (%), respectively. Moreover, the $(Y_{0.90}Eu_{0.10})VO_4$ and $(Y_{0.95}Dy_{0.05})VO_4$ film exhibit vivid red color and bright green color under UV excitation at 254 nm.

Author Contributions: Conceptualization, T.C. and H.Z.; methodology, X.W.; software, T.C.; validation, Z.L. and J.L.; formal analysis, X.W.; investigation, T.C.; resources, X.W.; data curation, Z.L.; writing—original draft preparation, T.C.; writing—review and editing, X.W.; visualization, X.W.; supervision, X.W.; project administration, X.W.; funding acquisition, X.W. and J.L. All authors have read and agreed to the published version of the manuscript.

Funding: This work was financially supported by the Natural Science Foundation of China (No. 52062011, 51402059) and Natural Science Foundation of Guangxi Province (No. 2018GXNSFAA050011).

Institutional Review Board Statement: Not applicable.

Informed Consent Statement: Not applicable.

Data Availability Statement: Not applicable.

Conflicts of Interest: The authors declare no conflict of interest.

References

1. Dunlap-Shohl, W.A.; Zhou, Y.; Padture, N.P.; Mitzi, D.B. Synthetic Approaches for Halide Perovskite Thin Films. *Chem. Rev.* **2019**, *119*, 3193–3295. [[CrossRef](#)] [[PubMed](#)]
2. Liang, K.; Li, L.; Yang, Y. Inorganic Porous Films for Renewable Energy Storage. *ACS Energy Lett.* **2017**, *2*, 373–390. [[CrossRef](#)]
3. Liu, L.; Wang, S.; Zhao, B.; Pei, P.; Fan, Y.; Li, X.; Zhang, F. Er³⁺ Sensitized 1530 nm to 1180 nm Second Near-Infrared Window Upconversion Nanocrystals for In Vivo Biosensing. *Angew. Chem. Int. Ed.* **2018**, *57*, 7518–7522. [[CrossRef](#)] [[PubMed](#)]
4. Mashford, B.S.; Nguyen, T.L.; Wilson, G.J.; Mulvaney, P. All-inorganic quantum-dot light-emitting devices formed via low-cost, wet-chemical processing. *J. Mater. Chem. A* **2010**, *20*, 167–172. [[CrossRef](#)]
5. Vadivel, S.; Paul, B.; Kumaravel, M.; Hariganesh, S.; Rajendran, S.; Mantilaka, M.M.M.G.P.G.; Mamba, G.; Puviarasu, P. Facile synthesis of YbVO₄, and YVO₄ nanostructures through MOF route for photocatalytic applications. *Inorganic Chem. Commun.* **2020**, *115*, 107855. [[CrossRef](#)]
6. Yi, S.; Bae, J.S.; Shim, K.S.; Moon, B.K.; Jeong, J.H.; Chung, S.T.; Kim, J.H. Luminescence characteristics of Eu-doped GdVO₄ thin films grown by pulsed-laser deposition. *J. Vac. Sci. Technol. A* **2005**, *23*, 1124–1127. [[CrossRef](#)]
7. Xu, H.; Wang, H.; Jin, T.; Yan, H. Rapid fabrication of luminescent Eu: YVO₄ films by microwave-assisted chemical solution deposition. *Nanotechnology* **2005**, *16*, 65–69. [[CrossRef](#)]
8. Hou, Z.; Yang, P.; Li, C.; Wang, L.; Lian, H.; Quan, Z.; Lin, J. Preparation and Luminescence Properties of YVO₄:Ln and Y(V, P)O₄:Ln (Ln = Eu³⁺, Sm³⁺, Dy³⁺) Nanofibers and Microbelts by Sol-Gel/Electrospinning Process. *Chem. Mater.* **2008**, *20*, 6686–6696. [[CrossRef](#)]
9. Geng, F.; Matsushita, Y.; Ma, R.; Xin, H.; Tanaka, M.; Izumi, F.; Iyi, N.; Sasaki, T. General synthesis and structural evolution of a layered family of Ln₈(OH)₂₀Cl₄·nH₂O (Ln = Nd, Sm, Eu, Gd, Tb, Dy, Ho, Er, Tm, and Y). *J. Am. Chem. Soc.* **2008**, *130*, 16344–16350. [[CrossRef](#)]
10. Geng, F.; Xin, H.; Matsushita, Y.; Ma, R.; Tanaka, M.; Izumi, F.; Iyi, N.; Sasaki, T. New layered rare-earth hydroxides with anion-exchange properties. *Chem. Eur. J.* **2008**, *14*, 9255–9260. [[CrossRef](#)]
11. Gandara, F.; Perles, J.; Snejko, N.; Iglesias, M.; Gomez-Lor, B.; Gutierrez-Puebla, E.; Monge, M.A. Layered rare-earth hydroxides: A class of pillared crystalline compounds for intercalation chemistry. *Angew. Chem. Int. Ed.* **2006**, *45*, 7998–8001. [[CrossRef](#)] [[PubMed](#)]
12. McIntyre, L.J.; Jackson, L.K.; Fogg, A.M. Ln₂(OH)₅NO₃ · xH₂O (Ln = Y, Gd-Lu): A Novel Family of Anion Exchange Intercalation Hosts. *Chem. Mater.* **2008**, *20*, 335–340. [[CrossRef](#)]
13. Hindocha, S.A.; McIntyre, L.J.; Fogg, A.M. Precipitation synthesis of lanthanide hydroxy nitrate anion exchange materials, Ln₂(OH)₅NO₃·H₂O (Ln = Y, Eu-Er). *J. Solid State Chem.* **2009**, *182*, 1070–1074. [[CrossRef](#)]
14. Gandara, F.; Puebla, E.G.; Iglesias, M.; Proserpio, D.M.; Snejko, N.; Monge, M.A. Controlling the structure of Arenedisulfonates toward Catalytically Active Materials. *Chem. Mater.* **2009**, *21*, 655–661. [[CrossRef](#)]
15. Sokolov, M.R.; Enakieva, Y.Y.; Yapyrintsev, A.D.; Shiryaev, A.A.; Zvyagina, A.I.; Kalinina, M.A. Intercalation of Porphyrin-Based SURMOF in Layered Eu (III) Hydroxide: An Approach Toward Symbiotic Hybrid Materials. *Adv. Funct. Mater.* **2020**, *30*, 2000681. [[CrossRef](#)]
16. Lee, K.H.; Lee, B.I.; You, J.; Byeon, S.H. Transparent Gd₂O₃:Eu phosphor layer derived from exfoliated layered gadolinium hydroxide nanosheets. *Chem. Commun.* **2010**, *46*, 1461–1463. [[CrossRef](#)]
17. Zhao, Y.; Li, J.; Guo, M.; Yang, X. Structural and photoluminescent investigation of LTbH/LEuH nanosheets and their color-tunable colloidal hybrids. *J. Mater. Chem. C* **2013**, *1*, 3584–3592. [[CrossRef](#)]
18. Hu, L.; Ma, R.; Ozawa, T.C.; Sasaki, T. Exfoliation of layered europium hydroxide into unilamellar nanosheets. *Chem. Asian J.* **2010**, *5*, 248–251. [[CrossRef](#)]
19. Zhu, Q.; Li, J.; Zhi, C.; Li, X.; Sun, X.; Sakka, Y.; Golberg, D.; Bando, Y. Layered Rare-Earth Hydroxides (LRHs) of (Y_{1-x}Eu_x)₂(OH)₅NO₃·nH₂O (x = 0–1): Structural Variations by Eu³⁺ Doping, Phase Conversion to Oxides, and the Correlation of Photoluminescence Behaviors. *Chem. Mater.* **2010**, *22*, 4204–4213. [[CrossRef](#)]
20. Wu, X.; Li, J.; Zhu, Q.; Li, J.; Ma, R.Z.; Sasaki, T.; Li, X.; Sun, X.; Sakka, Y. The effects of Gd³⁺ substitution on the crystal structure, site symmetry, and photoluminescence of Y/Eu layered rare-earth hydroxide (LRH) nanoplates. *Dalton Trans.* **2012**, *41*, 1854–1861. [[CrossRef](#)]
21. Wu, X.; Li, J.; Zhu, Q.; Liu, W.; Li, J.; Li, X.; Sun, X.; Sakka, Y. One-step freezing temperature crystallization of layered rare-earth hydroxide (Ln₂(OH)₅NO₃·nH₂O) nanosheets for a wide spectrum of Ln (Ln = Pr-Er, and Y), anion exchange with fluorine and sulfate, and microscopic coordination probed via photoluminescence. *J. Mater. Chem. C* **2015**, *3*, 3428–3437. [[CrossRef](#)]
22. Hu, L.; Ma, R.; Ozawa, T.C.; Sasaki, T. Oriented Monolayer Film of Gd₂O₃:0.05Eu Crystallites: Quasi-Topotactic Transformation of the Hydroxide Film and Drastic Enhancement of Photoluminescence Properties. *Angew. Chem. Int. Ed.* **2009**, *48*, 3846–3849. [[CrossRef](#)] [[PubMed](#)]

23. Zhu, Q.; Li, J.; Zhi, C.; Ma, R.; Sasaki, T.; Xu, J.; Liu, C.; Li, X.; Sun, X.; Sakka, Y. Nanometer-thin layered hydroxide platelets of $(Y_{0.95}Eu_{0.05})_2(OH)_5NO_3 \cdot xH_2O$: Exfoliation-free synthesis, self-assembly, and the derivation of dense oriented oxide films of high transparency and greatly enhanced luminescence. *J. Mater. Chem.* **2011**, *21*, 6903–6908. [[CrossRef](#)]
24. Huang, J.; Zhang, T.; Ren, K.; Zhang, R.; Wu, X.; Li, J. Fabrication of oriented oxide films from exfoliated yttrium hydroxide layers: Enhanced photoluminescence and unexplored behavior of energy transfer. *J. Alloys Compd.* **2018**, *763*, 815–821. [[CrossRef](#)]
25. Chu, N.; Sun, Y.; Zhao, Y.; Li, X.; Sun, G.; Ma, S.; Yang, X. Intercalation of organic sensitizers into layered europium hydroxide and enhanced luminescence property. *Dalton Trans.* **2012**, *41*, 7409–7414. [[CrossRef](#)]
26. Sun, Y.; Chu, N.; Gu, Q.; Pan, G.; Sun, G.; Ma, S.; Yang, X. Hybrid of Europium-Doped Layered Yttrium Hydroxide and Organic-Sensitizer Effect of Solvent on Structure and Luminescence Behavior. *Eur. J. Inorg. Chem.* **2013**, 32–38. [[CrossRef](#)]
27. Wu, X.; Li, J.; Li, J.; Zhu, Q.; Li, X.; Sun, X.; Sakka, Y. Layered rare-earth hydroxide (LRH) and oxide nanoplates of the Y/Tb/Eu system: Phase controlled processing, structure characterization, and color-tunable photoluminescence via selective excitation and efficient energy transfer. *Sci. Technol. Adv. Mater.* **2013**, *14*, 015006. [[CrossRef](#)]
28. Wu, X.; Li, J.; Ping, D.; Li, J.; Zhu, Q.; Li, X.; Sun, X.; Sakka, Y. Structure Characterization and Photoluminescence Properties of $(Y_{0.95-x}Gd_xEu_{0.05})_2O_3$ Red phosphors Converted from Layered Rare-Earth Hydroxide (LRH) nanoflake precursors. *J. Alloys Compd.* **2013**, *559*, 188–195. [[CrossRef](#)]
29. Liu, S.; Li, J.; Liu, W.; Cui, H.; Liu, M.; Chen, J.; Zhu, H.; Li, X.; Sun, X. A novel method for improving particle growth and photoluminescence through F- substituting for gallery NO_3^- in layered Y./Eu hydroxides. *Chem. Eng. J.* **2020**, *380*, 122618. [[CrossRef](#)]
30. Zhu, Q.; Li, J.; Li, X.; Sun, X.; Yang, Q.; Zhu, M.; Sakka, Y. Tens of micron-sized unilamellar nanosheets of Y/Eu layered rare-earth hydroxide: Efficient exfoliation via fast anion exchange and their self-assembly into oriented oxide film with enhanced photoluminescence. *Sci. Technol. Adv. Mater.* **2014**, *15*, 506–512. [[CrossRef](#)]
31. Hu, L.; Ma, R.Z.; Ozawa, T.C.; Geng, F.; Lyi, N.B.; Sasaki, T. Oriented films of layered rare-earth hydroxide crystallites self-assembled at the hexane/water interface. *Chem. Commun.* **2008**, *40*, 4897–4899. [[CrossRef](#)] [[PubMed](#)]
32. Yoon, Y.S.; Byeon, S.H.; Lee, I.S. Unexplored thermal transformation behavior of two-dimensionally bound gadolinium hydroxide layers: Fabrication of oriented crystalline films of gadolinium oxychloride nanosheets suitable for the multicolor luminescence with color tunability. *Adv. Mater.* **2010**, *22*, 3272–3276. [[CrossRef](#)] [[PubMed](#)]
33. Lee, B.I.; Lee, E.S.; Byeon, S.H. Assembly of layered rare-earth hydroxide nanosheets and SiO_2 nanoparticles to fabricate multifunctional transparent films capable of combinatorial color generation. *Adv. Funct. Mater.* **2012**, *22*, 3562–3569. [[CrossRef](#)]
34. Zhu, Q.; Li, S.; Wang, Q.; Qi, Y.; Li, X.; Sun, X.; Li, J. Grafting of terbium(iii) complexes onto layered rare-earth hydroxide nanosheets to fabricate novel optical fiber temperature sensors. *Nanoscale* **2019**, *11*, 2795. [[CrossRef](#)]
35. Liu, L.; Yu, M.; Zhang, J.; Wang, B.; Liu, W.; Tang, Y. Facile fabrication of color-tunable and white light emitting nano-composite films based on layered rare-earth hydroxides. *J. Mater. Chem. C* **2015**, *3*, 2326–2333. [[CrossRef](#)]
36. Wang, Z.; Li, J.; Zhu, Q.; Li, X.; Sun, X. Sacrificial conversion of layered rare-earth hydroxide (LRH) nanosheets into $(Y_{1-x}Eu_x)PO_4$ nanophosphors and investigation of photoluminescence. *Dalton Trans.* **2016**, *45*, 5290–5299. [[CrossRef](#)]
37. Huang, S.; Wang, Z.; Zhu, Q.; Shi, X.; Wang, X.; Li, X.; Sun, X.; Li, J. A new protocol for templated synthesis of YVO_4 : Ln luminescent crystallites (Ln = Eu, Dy, Sm). *J. Alloys Compd.* **2019**, *776*, 773–781. [[CrossRef](#)]
38. Xu, W.; Wang, Y.; Bai, X. Controllable synthesis and size-dependent luminescent properties of $YVO_4:Eu^{3+}$ nanospheres and microspheres. *J. Phys. Chem. C* **2010**, *114*, 14018–14024. [[CrossRef](#)]
39. Yang, X.; Zhang, Y.; Xu, L.; Zhai, Z.; Li, M.; Li, M.; Liu, X.; Hou, W. Surfactant-free sacrificial template synthesis of submicrometer-sized $YVO_4:Eu^{3+}$ hierarchical hollow spheres with tunable textual parameters and luminescent properties. *Dalton Trans.* **2013**, *42*, 3986–3993. [[CrossRef](#)]
40. Jia, G.; Song, Y.; Yang, M. Uniform $YVO_4:Ln^{3+}$ (Ln = Eu, Dy, and Sm) nanocrystals: Solvothermal synthesis and luminescence properties. *Opt. Mater.* **2009**, *31*, 1032–1037. [[CrossRef](#)]
41. Judd, B.R. Optical absorption intensities of rare-earth ions. *Phys. Rev.* **1962**, *127*, 750. [[CrossRef](#)]
42. Ofelt, G.S. Intensities of crystal spectra of rare-earth ions. *J. Chem. Phys.* **1962**, *37*, 511–520. [[CrossRef](#)]